Volume 1 | Number 1 | Jan 2013 | Pages 1–100

Journal of
Materials Chemistry A

Materials for energy and sustainability
www.rsc.org/materialsA

Li⁺

ROYAL SOCIETY
OF CHEMISTRY

ROYAL SOCIETY
OF CHEMISTRY

www.rsc.org/materialsA

Journal of Materials Chemistry A

PAPER

Graphene hydrogels functionalized non-covalently by Alizarin: an ideal electrode materials for symmetric supercapacitor

Ning An, Yufeng An, Zhongai Hu*, Bingshu Guo, Yuying Yang, Ziqiang Lei

In present work, the anthraquinone derivative Alizarin (AZ) with multi-electron redox center as the functionalizing molecule has been immobilized onto the three-dimensional (3D) self-assembled graphene hydrogels (SGHs) through non-covalent functionalization strategy. The excellent electrical conductivity and interconnected macroporous framework of SGHs facilitate unconstrained electrolyte ions diffusion and electron transportation. Moreover, the surface confined redox reactions and fast kinetic feature of AZ molecules result in outstanding electrochemically capacitive performance. In the three-electrode system, the AZ-functionalized SGHs (AZ-SGHs) electrodes exhibit larger specific capacitance (as high as 350 F g^{-1} at 1 A g^{-1}, two times higher than bare SGHs) and ultrahigh rate capability (61 % capacitance retention at 200 A g^{-1}) in aqueous electrolyte solutions. More importantly, when the resultant AZ-SGHs electrodes are integrated a symmetric supercapacitor (SSC), the electrode material shows a good self-synergy and potential self-matching behavior due to two pairs of redox peaks with mirror symmetry. As the result, the AZ-SGHs SSC exhibits an excellent energy storage performance. At a voltage range from 0 to 1.4 V, a maximum energy density of 18.2 W h kg^{-1} is achieved at a power density of 700 W kg^{-1}.

1. Introduction

Supercapacitors, also known as electrochemical capacitors, are considered as supreme candidate of sustainable energy storage/conversion systems because of high power density, exceptionally long cycle life and environmental friendliness.[1-4] However, the intrinsically low energy density of double-layer energy storage mechanism limits their large-scale industrialization.[5] To achieve the high energy density of electrochemical capacitors while maintaining their exclusively high power density, the nanostructured pseudocapacitive materials such as various transition-metal oxides[6-11] and conducting polymers [12-14] have been extensively studied. Unfortunately, the sources of these materials are limited and still relatively expensive. Furthermore, nanostructured materials with a particular architecture need complex material engineering which also is an unfavorable factor for the large-scale commercialization.[15] As a new type of electrode material, organic molecules with electrochemical reversibility have exhibited the potential to bridge the gap between high energy density and power density.[16] Compared with the transition-metal based pseudocapacitive materials, organic molecules are derived from low-cost, green and renewable resources and they can possess considerable energy density owing to the multi-electron Faradaic reactions in a low-molecular-weight charge storage unit.[17]

More importantly, their electrochemical properties can be reasonably tuned through the special organic functional groups and molecular structures,[18] which is absent for most of inorganic electrode materials. Among numerous organic molecules, quinone compounds have shown up prominently as electrode materials for energy storage devices owing to excellently electrochemical reversibility and stability.[19-21] However, these quinone molecules with the poor electroconductivity are hard to release electrochemical capacitance when they are used alone. In order to address this problem, the organic redox centers have been anchored onto conductive substrates and/or incorporated into conductive hosts, particularly on carbonaceous materials, as stationary phase.[22-25]

Recently, graphene hydrogels, a new kind of graphene materials, have attracted considerable interest owing to their inter-connected 3D macroporous framework and excellent electrical conductivity (10^6 S cm^{-1}). Compared with traditional 2D plane graphene, graphene hydrogels possess larger specific surface areas and provide continuous electron transport channel because they can effectively prevent the agglomeration or re-stack between graphene sheets caused by the strong π-π interaction. [26] We can not only utilize its defects or residual groups to immobilize organic molecules on graphene sheets through covalent modification,[27] but also rely on van der Waals forces, electrostatic interactions and/or π-π stacking to attach organic molecules on the graphene hydrogels backbone.[28] Indeed, covalent functionalization of carbon substrates would inevitably destroy the conjugate structure of graphene by conversion of carbon atoms from sp^2 to sp^3 hybridization and then decrease the electrical conductivity by one to several order of magnitudes.[29] Comparatively, non-covalent functionalization

*Key Laboratory of Eco-Environment-Related Polymer Materials of Ministry of Education, Key Laboratory of Polymer Materials of Gansu Province, College of Chemistry and Chemical Engineering, Northwest Normal University, Lanzhou, Gansu 730070, China. Fax: +86 931 8859764; Tel.: +86 931 7973255; E-mail: zhongai@nwnu.edu.cn

without disrupting the sp^2 network of graphene is more useful as a means in high-performance electrode materials of electrochemical capacitors.[30]

In the present work, we used a multi-redox anthraquinone derivative Alizarin (AZ) molecule to modify the 3D self-assembled graphene hydrogels (SGHs) by the non-covalent functionalization. In the three-electrode system, the resultant AZ-SGHs electrode shows two pairs of mirror symmetry reversible peaks in the positive (*ca.* +0.83 V) and negative potential region (*ca.* -0.18 V), respectively, because two types of organic functional groups (hydroxyl and carbonyl) of AZ provide two multi-electron redox centers during the electrochemical process. The further measurements indicate that the resultant electrode exhibits excellent capacitive performances in term of wide voltage window (1.4 V in 1 mol L^{-1} H$_2$SO$_4$ solution), larger specific capacitance (as high as 350 F g^{-1} at 1 A g^{-1}, two times higher than bare SGHs) and ultrahigh rate capability (the specific capacitance at 200 A g^{-1} is 61% of it at 1 A g^{-1}). More importantly, when the resultant AZ-SGHs electrodes are integrated a symmetric supercapacitor, the electrode material shows a good self-synergy and potential self-matching behavior. As the result, the integrated devices not only deliver higher energy density (18.2 W h kg^{-1} at 700 W kg^{-1}) compared with other symmetric supercapacitors (<10 Wh kg^{-1}) in aqueous electrolyte solutions but also exhibit extraordinary rate capability with 64% of specific capacitance retained when the current density increased from 1 to 50 A g^{-1}.

2. Experimental

2.1. Materials

Ascorbic acid (Vc), sulfuric acid (98%, H$_2$SO$_4$), acetone were purchased from Sinopharm Chemical Reagent Corp (China). Alizarin was purchased from Alfa-Aesar. All the experiments were carried out using deionized (DI) water and analytical reagent. GO was prepared from pure graphite powder by a modification of Hummers method.[31, 32]

2.2. Sample preparation

2.2.1. Synthesis of SGHs

100 mL homogeneous GO solution (1.6 mg mL^{-1}) and 0.1 g Vc were pre-mixed and sealed in a 100mL Teflon-lined autoclave maintained at 180 °C for 12h. After the autoclave was naturally cooled down to room temperature, the prepared gel was repeatedly washed with DI water and freeze-dried.

2.2.2. Synthesis of AZ-SGHs

The certain amount of as-received organic compound (AZ) was dissolved in 50 mL acetone and then 0.1 g SGHs was added under sonication 5 min. After that, the mixture was allowed to stand for 12 h to immobilize AZ molecules on the SGHs surface. Finally, by evaporating the acetone at 70 °C, the organic compound was anchored on the surface of carbon material. For the convenience of description, the products were denoted as AZ-SGHs x:y to indicate the mass ratio of AZ (x) to SGHs (y).

2.3. Characterization of samples

The morphologies of products were observed by field-emission scanning electron microscope (FESEM; ULTRA Plus, Germany) and transmission electron microscope (TEM; JEM-2010, Japan). Powder

X-ray diffraction (XRD) patterns were implemented on a diffractometer (D/Max-2400, Rigaku) using Cu Kα radiation (λ = 1.5418 Å) at 40 kV, 100 mA. Fourier-transform infrared spectroscopy (FT-IR) spectra were analyzed by a Nicolet Nexus 670 spectrometer. Ultraviolet–visible spectroscopy (UV-vis) detections were performed on a UV-1102 spectrophotometer. The Brunauer-Emmett-Teller (BET) surface areas of the samples were analyzed by nitrogen adsorption in a Micromeritics ASAP 2020 nitrogen adsorption apparatus (U.S.A.). Raman spectra were recorded with an inVia Raman spectrometer (Renishaw) with an argon ion laser (λ = 514 nm). The conductivities of samples were measured by a four-probe conductivity meter (SX1944) at room temperature. Chemical state analyses of samples were performed by X-ray photoelectron spectroscopy (XPS; Escalab 210 system, Germany) with a monochromatic Al Kα radiation source (ThermoVG Scientific).

2.4. Electrochemical measurement

In the three-electrode system, the platinum foil and saturated calomel electrode (SCE) were used as the counter electrode and reference electrode, respectively. The working electrode was fabricated according to the literature.[33] Typically, the electrode material (16 mg) and acetylene black (weight ratio of 85:15) were completely dispersed into 0.4 mL Nafion solution (0.25 wt %) by sonication. Then 5 μL above suspension using a pipet gun was dropped onto the glassy carbon electrode (5 mm) with the mass of 1.0 mg cm^{-2} and completely dried at room temperature.

The capacitive performances of supercapacitor were tested in the two-electrode system, in which the positive and negative electrodes were separated by a glass-fiber. The cyclic voltammetry (CV), galvanostatic charge-discharge and electrochemical impedance spectroscopy (EIS) tests were all investigated in 1 M H$_2$SO$_4$ with a CHI 760E electrochemical workstation (Chenghua, Shanghai, China).

3. Results and discussion

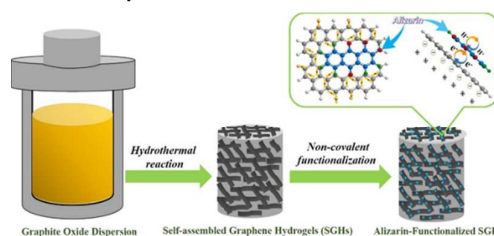### 3.1 The formation process of AZ-SGHs

Fig. 1 The formation process of AZ-SGHs electrode material.

The formation process of AZ-SGHs electrode material is outlined in Fig. 1. Firstly, graphite oxide (GO) sheets were ultrasonically dispersed in 100 mL DI water. Through hydrothermal reduction, the GO sheets become locally hydrophobic due to most of the surface oxygenic functional groups were removed. Under the influence of electrostatic repulsion, hydrophobicity and π-π stacking interactions, the flexible graphene sheets coalesce and overlap with each other, which forms the physical cross-links sites of the 3D graphene hydrogels network.[34, 35] Finally, through non-covalent functionalization, AZ molecules were immobilized onto the SGHs framework without disrupting the sp^2 network of graphene. The resulting composite is suitable for releasing the electrochemical capacitance of AZ molecules as 3D graphene macroporous

framework provides continuous charge transfer pathways to allow unconstrained electron transport and electrolyte ions diffusion.

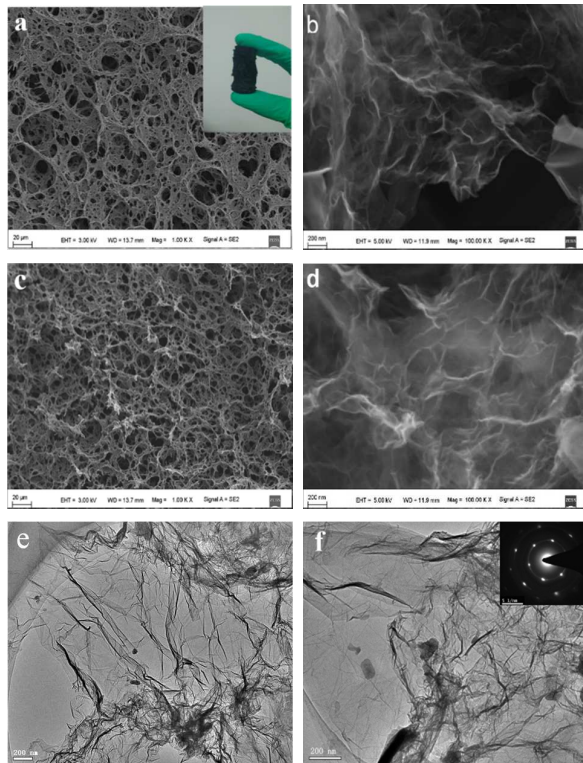## 3. 2 Physical characterizations

Fig. 2 (a and b) SEM images and photograph (insert) of SGHs; (c and d) SEM images of AZ-SGHs 3:5 at different magnification; (e) TEM images of SGHs and (f)AZ-SGHs 3:5 and the electron diffraction pattern (insert).

The surface morphologies of SGHs and AZ-SGHs 3:5 were imaged by SEM. As shown in Fig. 2a, the freeze-dried SGHs have an interconnected 3D macroporous framework with pore sizes ranging from sub-micrometers to several micrometers. The ultrathin and flexible nature of graphene sheets can be clearly observed in the high magnification SEM image (Fig. 2b). The N_2 adsorption/desorption isotherm of SGHs (Figure S1) displays a typical type-IV behavior with the specific surface area of 215 m^2 g^{-1}. The obvious hysteresis loop in the range of P/P$_0$=0.4-0.9 and the sharp increase of the adsorption amount at P/P$_0$>0.9 indicate the existence of a large number of mesopores and macropores in SGHs.[36] The SEM images of AZ-SGHs 3:5 (Figure 2c and d) maintain the 3D framework network of the precursor SGHs. Therefore, non-covalent functionalization strategy does not influence SGHs morphology. Fig. 2e and f show the TEM images of SGHs and AZ-SGHs 3:5, which can be seen that graphene sheets with some wrinkles are almost transparent under TEM electron irradiation. The electron diffraction pattern (Fig. 2f insert) further confirms the production of high-quality graphene sheets.[37]
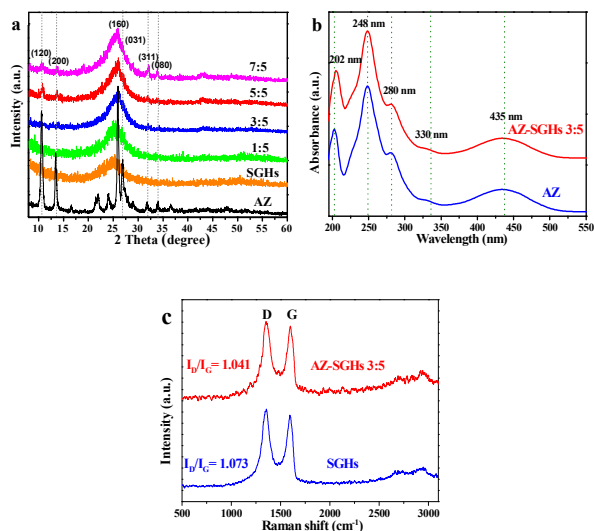

Fig. 3 (a) XRD patterns of pure AZ, SGHs and AZ-SGHs composites with different mass ratios of AZ (x) to SGHs (y), (b) UV-vis absorption spectra of pure AZ and AZ-SGHs 3:5 composite and (c) Raman spectra of SGHs and AZ-SGHs 3:5.

The crystal structures of AZ, SGHs and AZ-SGHs composites were studied by the XRD analysis. As shown in Fig. 3a, the diffraction peaks at 2ϑ of 10.72, 13.48, 26.04, 26.90, 31.81, and 33.66° which can be distinctly indexed as (120), (200), (160), (031), (311), and (080) crystalline plane of AZ (JCPDS PDF No. 14-0887), respectively. The broad XRD peak of the SGHs at 2ϑ=25.3° indicates the poor ordering of graphene sheets along their stacking direction and reflects that the framework of SGHs is composed of few-layer stacked graphene sheets, which is consistent with the SEM and TEM. As the AZ content increases, the XRD patterns of AZ-SGHs composites (5:5 and 7:5) show the AZ characteristic peaks. This result confirms that AZ molecules were immobilized on the surface of SGHs. UV-vis absorption spectra of the AZ and AZ-SGHs 3:5 were performed (Fig. 3b). For AZ, two obvious bands appearing at 202 and 248 nm are ascribed to the π-σ* and π-π* transition of the benzenoid system, respectively.[21] Shoulder and extremely weak absorption (280 nm and 330 nm) at the longer wavelength side are assigned to quinonoid π-π* transitions. The absorption band at 435 nm is attributed to C=O bond of quinoid form.[38] For AZ-SGHs composites, the absorption peak of π-σ* transition (*ca.* 205 nm) shows a 3 nm red shift compared with AZ, suggesting AZ was anchored on the surface of graphene sheet via strong π–π stacking interaction.[39] On the FT-IR spectra of the AZ and AZ-SGHs composites (Fig. S2), we can see that the spectra of samples show a strong similarity in their main characteristic IR bands, strongly confirming the existence of AZ molecules on the conductive substrate. The band at around 1640 cm^{-1} corresponding to C=O stretching vibrations of the quinonyl group, and the intensive bands at 713 and 1283 cm^{-1} are ascribed to the aromatic C-H out-of-plane deformation vibration and C-O skeletal vibration, respectively. Besides, the bands of COH in-plane bending vibration and typical aromatic skeleton stretching vibration are revealed at 1459 cm^{-1} and 1590 cm^{-1}.[19, 40]

Raman spectroscopy is an efficient tool to investigate electronic properties of carbon materials, particularly for distinguishing ordered and disordered crystal structures.[41] As illustrated in Fig. 3c,

This journal is © The Royal Society of Chemistry year

J. Mater. Chem. A, [year], **[vol.]**, 00-00 | **3**

the SGHs contains both D and G bands. It is generally accepted that D band is assigned to the presence of structure defects and disorders in carbon systems while G band is attributed to the stretching vibration of any pair of sp^2 sites inside the graphitic pattern.[42] Therefore, the integrated intensity ratio between the D-band and G-band (I_D/I_G) is often used to manifest the extent of microstructural disorder, which is inversely proportional to the crystallite size of graphene.[43] The I_D/I_G values of SGHs is about 1.073 which indicates that SGHs possess both localized graphitic structure and small amount of defects. The value of I_D/I_G for AZ-SGHs 3:5 is 1.041, smaller than SGHs, which further confirms that the non-covalent functionalization strategy can effectively preserve the conjugated structure of graphene.
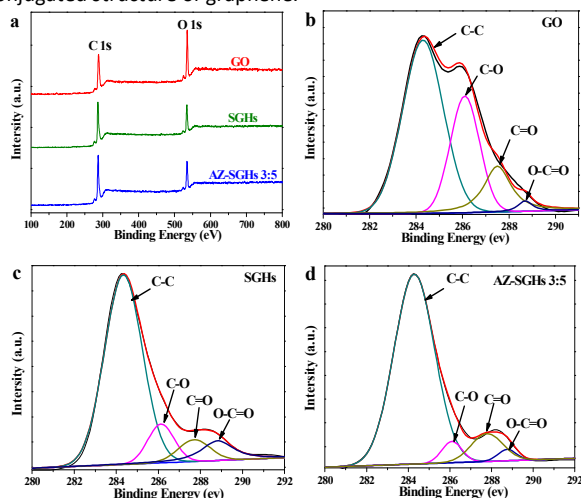

Fig. 4 XPS spectra of the survey scan (a); C 1s region of GO (b), SGHs (c), AZ-SGHs 3:5 composite (d), respectively.

As Fig. 4a shows, the XPS spectra of graphite oxide (GO), SGHs and AZ-SGHs 3:5 all demonstrate a principal C1s peak (~284.4 eV) and a pronounced O1s peak (~535.5 eV) without evidence of impurities. Fig. 4b-d gives the high-resolution C1s spectra of samples as well as their decompositions. Obviously, the C1s spectrum of GO can be fitted by four peaks corresponding to different functional groups of carbon atoms: 284.4 eV (C-C), 286.2 eV (C-O), 287.7 eV (C=O), and 288.8 eV (O-C=O).[44] After reduction, these absorbance peaks greatly weakened because most of the surface oxygenic functional groups on the SGHs were successfully removed.[45] Compared with SGHs, the C1s XPS spectrum of AZ-SGHs 3:5 (Fig. 4c) exhibits a more well-defined peak at 287.7 eV, which may be attributed to the C=O of AZ molecules on the surface of SGHs.
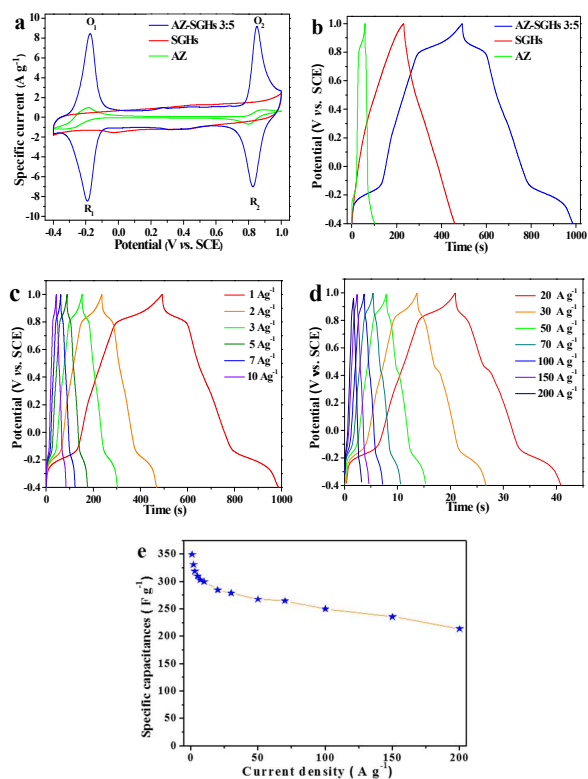
3.2 Electrochemical measurements

Fig. 5 (a) CV curves of SGHs, AZ and AZ-SGHs 3:5 at a scan rate of 5 mV s^{-1}, (b) galvanostatic charge/discharge curves of samples at 1 A g^{-1}, (c and d) galvanostatic charge-discharge curves of AZ-SGHs 3:5 at different current densities and (e) specific capacitances of AZ-SGHs 3:5 electrode at various current densities.

The electrochemical performances of samples were estimated using CV and galvanostatic charge-discharge tests in the three-electrode system. Fig. 5a shows the CV curves of SGHs, AZ and AZ-SGHs 3:5 electrodes at a potential of -0.4 to 1.0 V in 1 M H_2SO_4 as electrolyte. It can be seen that the CV curve of SGHs shows a typical rectangular shape, implying electrical double-layer energy storage mechanism. Comparatively, the AZ-SGHs 3:5 electrode exhibits a larger integral area than that of pure AZ and SGHs electrode, suggesting the significantly enhanced charge storage capability of composite. Particularly, the CV curve of AZ-SGHs 3:5 is characterized by two pairs of reversible peaks with mirror symmetry, O_1/R_1 couple and O_2/R_2 couple at approximately -0.18 and +0.83 V, respectively. The former peaks correspond to a reversible 2-electron redox of the 9, 10-quinone functional groups and the latter one also involves two electrons reaction which relates to the redox of 1, 2-dihydroxyl groups at more positive potentials.[46-48] The two pair redox peaks of AZ-SGHs electrode have nearly symmetrical wave-shapes and small peak separation (*ca.* 30 mV), indicating that the surface confined redox reactions have a good reversibility and fast charge transfer process. With increasing the scan rate, a weak irreversible reduction peak, designated as R_3, appeared at about +0.42 V (Fig. S3), which may be related to the production of AZ dimer.[49] Fig. 5b shows the galvanostatic charge-discharge curves of samples in the potential range from -0.4 to 1.0 V at 1 A g^{-1}. The potential-time curve of AZ-SGHs electrode shows two pairs of symmetrical charge-discharge voltage plateaus, which is consistent with the results of CV curves. Comparatively, the

This journal is © The Royal Society of Chemistry year

J. Mater. Chem. A, [year], **[vol.]**, 00-00 | **4**

galvanostatic charge-discharge curve of SGHs exhibits an ideal isosceles triangle, which is another characteristic of electrical double-layer behavior. The specific capacitance of AZ-SGHs 1:5, 3:5, 5:5, 7:5 at 1 A g^{-1} are 240, 350, 275, 272 F g^{-1}, respectively (Fig. S4), which are all much larger than that of the SGHs (162 F g^{-1}) and pure AZ (31 F g^{-1}). It is noteworthy that the specific capacitance of AZ-SGHs composite electrode decreases when the mass ratio of AZ to SGHs exceeds 3:5. This is probably because too much AZ molecules on the surface of graphene sheets will reduce the conductivity of composite. Based on the experimental results, the optimal mass ratio of AZ to SGHs for specific capacitance is 3:5. Fig. 5c and d shows galvanostatic charge-discharge curves of AZ-SGHs 3:5 at various specific currents. The relationship between specific capacitance and current density is illustrated in Fig. 5e. The maximum specific capacitance of AZ-SGHs 3:5 is calculated to be 350 F g^{-1} at 1 A g^{-1} and still retains at 61.1% at 200 A g^{-1}. This prominent rate capability is related to fast Faradaic reaction of AZ and inter-connected 3D macroporous structure which allow unconstrained electrolyte ions diffusion and electron transport. To the best of our knowledge, such rate capability is comparable or superior to the best results reported in the relative literature as shown in Table 1. The conductivity of the electrode materials was measured by a four-probe method. Pure AZ sample is almost non-conductive. Comparatively, AZ-SGHs 3:5 shows a higher conductivity of around 3.69 S cm^{-1} (4.25 S cm^{-1} of SGHs), which is in agreement with the CV and galvanostatic charge-discharge results.
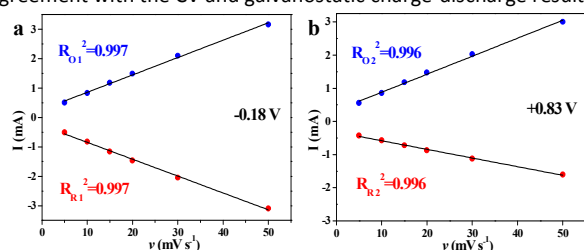

Fig. 6 The relationship between the peak current (*I*) of two pairs of redox peaks (a. -0.18 V and b. +0.83 V) and scan rate (*v*).

The analysis of relations between the peak current (*I*) and applied scan rate (*v*) can help us understand more about the kinetic information of electrode material. As shown in Fig.6, a reasonable linear relationship is observed between *I* and *v* for two pairs of redox peaks, indicating the redox sites are immobilized on the surface of the conductive substrate and this electrode reaction is not limited by concentration diffusion. This electrode kinetic behavior of AZ-SGHs is different from most pseudocapacitive metal oxide materials, where *I* varies with $v^{1/2}$ that is a diffusion-limited process.[52]

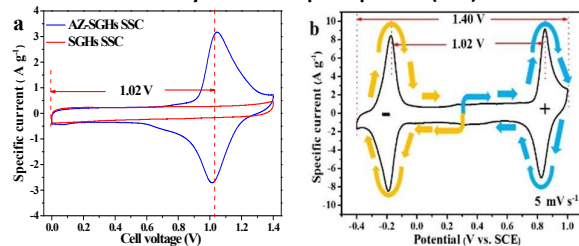### 3.3. Performances of symmetric supercapacitor (SSC)

Fig. 7 (a) CV curves for AZ-SGHs and SGHs SSC in 1 mol L^{-1} H$_2$SO$_4$ electrolyte; (b) CV curves of AZ-SGHs 3:5 electrodes in the three-electrode system at a scan rate of 5 mV s^{-1}.

It is well-known that the two-electrode system is suitable for the evaluation of actual supercapacitors performance. Based on the highly individual capacitive performance, as well as the good self-synergy and potential self-matching ability between the two redox centers of AZ-SGHs electrode, a novel symmetric capacitor has been assembled. Fig. 7a shows the CV curves of SGHs and AZ-SGHs SSC with cell voltage of 1.4 V at a scan rate of 10 mV s^{-1}. The CV curve of SGHs SSC exhibited a quasi-rectangular shape and no obvious redox peaks were observed, which is consistent with most literature reports.[53] As for the CV curve of AZ-SGHs SSC, its shape is very distinguished from that of the SGHs SSC, suggesting that its capacitance mainly originates from the electrochemical capacitance of AZ molecules. And a pair of well-defined and reversible redox peaks could be clearly observed with an anodic peak at around 1.01 V and a cathodic peak at about 1.04 V indicating excellent electrochemical reversibility and fast kinetic characteristic. Here a funny question is: why the CV curve of AZ-SGHs electrode has two pairs of reversible redox peaks in the three-electrode system but only one pair observed in the two-electrode system? To understand the electrochemical behavior for AZ-SGHs SSC, we should firstly start from the CV curve of AZ-SGHs electrode as shown in Fig. 7b. The two pairs of redox peaks at the potential of -0.18 and +0.83 V correspond to two half-reactions of AZ-SGHs, respectively. When the AZ-SGHs SSC begins charging, its cell voltage will start from 0 V and gradually increase. However, the potentials of positive and negative electrodes will begin from the relative value (where the state of electrodes corresponds to that at 0.3 V as shown in Fig. 7b) and shift positively and negatively respectively. In the initial charging stage, no obvious redox peak on the CV curve appears due to electrical double-layer behaviors. When the cell voltage of AZ-SGHs SSC reaches 1.02 V at charging segment, the oxidation reaction of O$_2$/R$_2$ couple occurs on the positive electrode while the reducing reaction of O$_1$/R$_1$ couple occurs on the negative electrode. And the two half-reactions superimpose on each other and emerge a pair of reversible redox peaks at 1.02 V in the two-electrode system. The variation of electrode states in the charging/discharging cycle is shown in Fig. 7b. This capability of the self-synergy and potential self-matching can make full use of the electrochemical capacitance of AZ-SGHs electrode in SSC device, which has not yet been reported in electrode material for supercapacitor.
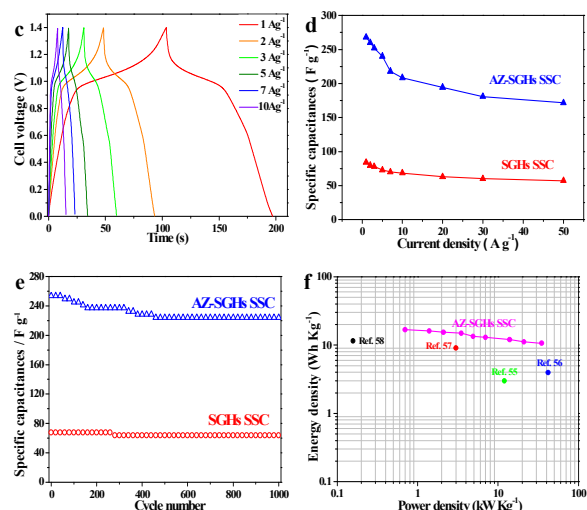
This journal is © The Royal Society of Chemistry year

J. Mater. Chem. A, [year], **[vol.]**, 00-00 | **5**
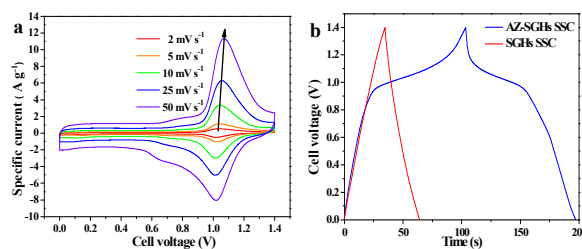
Fig. 8 (a) CV curves of AZ-SGHs SSC at different scan rates in 1 M H_2SO_4 aqueous solution, (b) galvanostatic discharge curves of AZ-SGHs and SGHs SSCs in 1 M H_2SO_4 electrolyte at 1 A g^{-1}, (c) galvanostatic discharge curves and (d) specific capacitances of AZ-SGHs SSC at various specific current, (e) cycling stability and Ragone plot (f) of AZ-SGHs SSC.

Fig. 8a shows the CV curves of AZ-SGHs SSC at scan rates from 2 to 50 mV s^{-1}. When increasing the scan rate, the curve shapes nearly keep unchanged, which reveals an excellent capacitance behavior and the fast diffusion of electrolyte ions into the graphene hydrogels network. It's worth noting that there is a weak irreversible reduction peak at around 0.7 V corresponding to an irreversible reaction of AZ dimer. This result is consisted with the CV curve of AZ-SGHs electrode in the three-electrode system. The galvanostatic charge/discharge curves of AZ-SGHs and SGHs SSC at 1 A g^{-1} are shown in Fig. 8b. Compared with SGHs SSC, the voltage-time curve of AZ-SGHs SSC has a symmetrical plateau at around 1.0 V, which indicates some contribution of the quick Faradaic reactions from AZ. The galvanostatic charge/discharge curves at different current densities from 1 A g^{-1} to 10 A g^{-1} are shown in Fig. 8c. The highly symmetrical charging-discharging characteristic indicates an excellent electrochemical reversibility. The relationship between current density and specific capacitance is illustrated in Fig. 8d. The gravimetric capacitance of AZ-SGHs SSC is as high as 285.6 F g^{-1} at a current density of 1 A g^{-1}, which is much higher than SGHs SSC(87.6 F g^{-1}). Furthermore, the AZ-SGHs SSC shows excellent rate performance with 63.2% of specific capacitance retained when the current density increased from 1 to 50 A g^{-1}. Moreover, the cycling stability of two capacitors is evaluated at 5 A g^{-1} for 1000 cycles (Fig. 8e). During the cycling, the AZ-SGHs SSC exhibits electrochemical stability with about 88% retention of the initial specific capacitance after 1000 cycles. Additionally, from the EIS analysis of AZ-SGHs SSC (Fig. S5) by applying frequency in the range of 0.01 kHz-100 kHz, the negligible semicircle in the high-frequency region and a nearly vertical line in the low-frequency region are detected, showing a small charge transfer resistance at the electrode/electrolyte interface and an obvious capacitive behavior with low diffusion resistance.[54] Fig. 8f is a Ragone plot, which correlates the energy and power densities of AZ-SGHs SSC. The maximum energy density is up to 18.2 W h kg^{-1} at a power density of 700 W kg^{-1}. It outperforms of SGHs SSC (*e.g.*, 5.1 W h kg^{-1} at 0.7 kW kg^{-1}) and most

of SSCs in the literature such as HPNCNTs//HPNCNTs (3 W h kg^{-1} at 12 kW kg^{-1}),[55] $Co(OH)_2$//$Co(OH)_2$ (3.96 W h kg^{-1} at 42 kW kg^{-1}),[56] Fe_3O_4/graphene//Fe_3O_4/graphene (9 W h kg^{-1} at 3 kW kg^{-1}),[57] Ni-Co oxide// Ni-Co oxide (11.5 W h kg^{-1} at 158 W kg^{-1}).[58]

4. Conclusion

In summary, this work provides a novel design idea to immobilize the multi-redox anthraquinone derivative AZ molecules on the surface of SGHs through non-covalent functionalization strategy. Base on the reversible multi-electron Faradaic reactions in organic molecules and effective 3D electron transport network of SGHs, the AZ-SGHs electrode material exhibits excellent capacitive performance such as larger specific capacitance and ultrahigh rate capability in aqueous electrolyte solutions. Furthermore, two redox active centers of the AZ-SGHs electrode exhibit the good self-synergy and potential self-matching ability in the SSC device, which leads to excellent energy storage performances. These encouraging discoveries can open up the possibility of multi-redox electrode materials for green and effective energy storage systems.
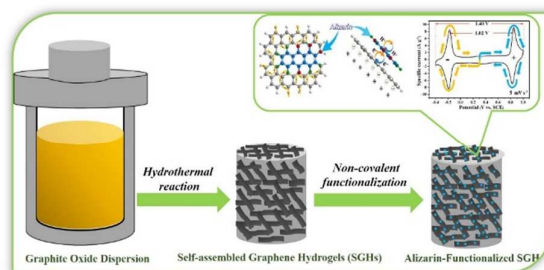
Acknowledgements

Notes and references

1 Z. Li, Z. Xu, H. Wang, J. Ding, B. Zahiri, C. M. B. Holt, X. Tan and D. Mitlin, Energy Environ. Sci., 2014, 7, 1708.
2 G. Wang, L. Zhang and J. Zhang, Chem. Soc. Rev., 2012, 41, 797.
3 Y. Gogotsi and P. Simon, Science, 2011, 334, 917.
4 J. Zhu, M. Chen, H. Wei, N. Yerra, N. Haldolaarachchige, Z. Luo, D. P. Young, T. C. Ho, S. Wei and Z. Guo, Nano Energy, 2014, 6, 180.
5 J. T. Zhang, J. W. Jiang, H. L. Li and X. S. Zhao, Energ. Environ. Sci., 2011, 4, 4009.
6 L. Li, Z. A. Hu, N. An, Y. Y. Yang and H. Y. Wu, J. Phys. Chem. C, 2014, 118, 22865.
7 W. Ji, J. Ji, X. Cui, J. Chen, D. Liu, H. Deng and Q. Fu, Chem. Commun., 2015, 51, 7669.
8 G. D. Moon, J. B. Joo, M. Dahl, H. Jung and Y. Yin, Adv. Funct. Mater., 2014, 24, 848.
9 H. Chen, L. Hu, M. Chen, Y. Yan and L. Wu, Adv. Funct. Mater., 2014, 24, 934.
10 H. Wang, Z. Xu, H. Yi, H. Wei, Z. Guo and X. Wang, Nano Energy, 2014, 7, 86.
11 J. Zhu, M. Chen, H. Qu, Z. Luo, S. Wu, H. A. Colorado, S. Wei and Z. Guo, Energy Environ. Sci., 2013, 6, 194.
12 Y. Zhao, H. Wei, M. Arowo, X. Yan, W. Wu, J. Chen, Y. Wang and Z. Guo, Phys. Chem. Chem. Phys., 2015, 17, 1498.
13 H. Wei, Y. Wang, J. Guo, X. Yan, R. O'Connor, X. Zhang, N. Z. Shen, B. L. Weeks, X. Huang, S. Wei and Z. Guo, ChemElectroChem, 2015, 2, 119.
14 C. Yang, H. Wei, L. Guan, J. Guo, Y. Wang, X. Yan, X. Zhang, S. Wei and Z. Guo, J. Mater. Chem. A, 2015, 3, 14929.
15 A. Jaffe, A. Saldivar Valde and H. I. Karunadasa, Chem. Mater., 2015, 27, 3568.

This journal is © The Royal Society of Chemistry year

J. Mater. Chem. A, [year], **[vol.]**, 00-00 | **6**

16 L. Madec, A. Bouvrée, P. Blanchard, C. Cougnon, T. Brousse, B. Lestriez, D. Guyomard and J. Gaubicher, Energ. Environ. Sci., 2012, 5, 5379.

17 T. Tomai, S. Mitani, D. Komatsu, Y. Kawaguchi and I. Honma, Sci. Rep., 2014, 4, 3591.

18 S. E. Burkhardt, M. A. Lowe, S. Conte, W. Zhou, H. Qian, G. G. Rodríguez-Calero, J. Gao, R. G. Hennig and H. D. Abruña, Energ. Environ. Sci., 2012, 5, 7176.

19 X. Chen, H. Wang, H. Yi, X. Wang, X. Yan and Z. Guo, J. Phys. Chem. C, 2014, 118, 8262.

20 H. Wang, H. Yi, C. Zhu, X. Wang and H. J. Fan, Nano Energy, 2015, 13, 658.

21 N. An, F. H. Zhang, Z. A. Hu, Z. M. Li, L. Li, Y. Y. Yang and Z. Q. Lei, RSC Adv., 2015, 5, 23942.

22 Z. Algharaibeh, P. G. Pickup, Electrochem. Commun., 2011, 13, 147.

23 G. Pognon, T. Brousse, L. Demarconnay and D. Bélanger, J. Power Sources, 2011, 196, 4117.

24 Z. Algharaibeh, X. Liu and P. G. Pickup, J. Power Sources, 2009, 187, 640.

25 N. An, Y. F. An, Z. A. Hu, Y. D. Zhang, Y. Y. Yang and Z. Q. Lei, RSC Adv., 2015, 5, 63624.

26 Y. Xu, K. Sheng, C. Li and G. Q. Shi, ACS Nano, 2010, 4, 4324.

27 Q. Wu, Y. Sun, H. Bai and G. Q. Shi, Phys. Chem. Chem. Phys., 2011, 13, 11193.

28 Y. Xu, Z. Lin, X. Huang, Y. Wang, Y. Huang and X. Duan, Adv. Mater., 2013, 25, 5779.

29 V. Georgakilas, M. Otyepka, A. B. Bourlinos, V. Chandra, N. Kim, K. C. Kemp, P. Hobza, R. Zboril and K. S. Kim, Chem. Rev., 2012, 112, 6156.

30 M. Jana, S. Saha, P. Khanra, P. Samanta, H. Koo, N. C. Murmu, and T. Kuila, J. Mater. Chem. A, 2015, 3, 7323.

31 Jr. W. S. Hummers and R. E. Offeman, J. Am. Chem. Soc., 1958, 80, 1339.

32 N. I. Kovtyukhova, P. J. Ollivier, B. R. Martin, T. E. Mallouk, S. A. Chizhik, E. V. Buzaneva, and A. D. Gorchinskiy, Chem. Mater., 1999, 11, 771.

33 S. Giri, D. Ghosh and C. K. Das, Adv. Funct. Mater., 2014, 24, 1312.

34 L. Zhang and G. Q. Shi, J. Phys. Chem. C, 2011, 115, 17206.

35 H. Wang, H. Yi, X. Chen and X. Wang, J. Mater. Chem. A, 2014, 2, 1165.

36 X. X. Xiang, Z. Z. Huang, E. Liu, H. J. Shen, Y. Y. Tian, H. Xie, Y. H. Wu and H. Z. Wu, Electrochim. Acta, 2011, 56, 9350.

37 Y. Zhao, C. G. Hu, Y. Hu, H. H. Cheng, G. Q. Shi and L. T. Qu, Angew. Chem., 2012, 124, 11533.

38 M. S. El Ezaby, T. M. Salem, A. H. Zewail and R. Issa, J Chem. Soc. B: Physical Organic, 1970, 1293.

39 G. E. Yuan, G. Zhang, J. Chen, L. Fu, L. Xu and F. Yang, J Solid State Electr., 2013, 17, 2711.

40 Z. Song, H. Zhan and Y. Zhou, Chem. Commun., 2009, 4, 448.

41 A. C. Ferrari and D. M. Basko, Nat. Nanotechnol., 2013, 8, 235.

42 A. Jänes, H. Kurig and E. Lust, Carbon, 2007, 45, 1226.

43 P. Hao, Z. Zhao, J. Tian, H. Li, Y. Sang, G. Yu, H. Cai, H. Liu, C. P. Wong and A. Umar, Nanoscale, 2014, 6, 12120.

44 Y. Zhou, G. Zhang, J. Chen, G. E. Yuan, L. Xu, L. Liu and F. Yang, Electrochem. Commun., 2012, 22, 69.

45 L. Tang, Y. Wang, Y. Li, H. Feng, J. Lu and J. Li, Adv. Funct. Mater., 2009, 19, 2782.

46 H. P. Dai and K. K. Shiu, Electrochim. Acta, 1998, 43, 2709.

47 K. R. Mahanthesha, B. K. Swamy, U. Chandra, Y. D. Bodke, K. V. K. Pai and B. S. Sherigara, Int. J. Electrochem. Sci., 2009, 4, 1237.

48 H. E. Zittel and T. M. Florence, Anal. Chem., 1967, 39, 320.

49 Y. C. Zhu and S. J. Dong, Acta Chim. Sinica, 1990, 48, 534.

50 H. Wang, H. Wu, Y. Chang, Y. Chen and Z. A. Hu, Chinese Sci. Bull., 2011, 56, 2092.

51 M. Jana, P. Khanra, N. C. Murmu, P. Samanta, J. H. Lee and T. Kuila, Phys. Chem. Chem. Phys., 2014, 16, 7618.

52 P. Simon, Y. Gogotsi and B. Dunn, Science, 2014, 343, 1210.

53 H. Peng, G. Ma, K. Sun, J. Mu and Z. Q. Lei, J. Mater. Chem. A, 2014, 2, 17297.

54 J. G. Wang, Y. Yang, Z. H. Huang and F. Kang, Carbon, 2013, 61, 190.

55 H. Wang, H. Yi, X. Chen and X. F. Wang, J. Mater. Chem. A, 2014, 2, 3223.

56 A. D. Jagadale, V. S. Kumbhar, D. S. Dhawale and C. D. Lokhande, Electrochim. Acta, 2013, 98, 32.

57 K. Karthikeyan, D. Kalpana, S. Amaresh and Y. S. Lee, RSC Adv., 2012, 2, 12322.

58 X. Lu, X. Huang, S. Xie, T. Zhai, C. Wang, P. Zhang, M. Yu, W. Li, C. Liang and Y. Tong, J. Mater. Chem. A, 2012, 22, 13357.

Table 1. Comparison of rate capability of different electrode materials.

Electrode material	Electrolyte	Potential window	Rate capability	Ref. (year)
Anthraquinone/carbon nanotubes	1 M H_2SO_4	-0.3 to -0.4 V (0.7 V)	59% at 20A g^{-1}	[19] (2014)
Anthraquinone/ porous graphitic carbon fibers	1 M H_2SO_4	-0.35 to 0.25 V (0.6 V)	57% at 60 A g^{-1}	[20] (2015)
2-Aminoanthraquinone functionalized graphene hydrogels	1 M H_2SO_4	-0.2 to 0.6 V (0.8 V)	58% at 90 A g^{-1}	[27] (2011)
Hydroquinone functionalized graphene hydrogels	1 M H_2SO_4	0 to 1.0 V (1.0 V)	20% at 20A g^{-1}	[28] (2013)
Sulfanilic acid azocromotrop modified RGO	2 M H_2SO_4	-0.6 to 1.0 V (1.6 V)	76% at 10A g^{-1}	[30] (2015)
Tert-butylhydroquinone-decorated graphene	1 M H_2SO_4	0 to 0.8 V (0.8 V)	63% at 8 A g^{-1}	[50] (2011)
6-Amino-4hydroxy-2-napthalenesulfonic acid modified RGO	1 M H_2SO_4	-1.0 to 1.0 V (2.0 V)	50% at 13 A g^{-1}	[51] (2014)
Alizarin-functionalized SGHs	1 M H_2SO_4	-0.4 to 1.0V (1.4V)	86% at 10 A g^{-1} 61% at 200 A g^{-1}	This work

This journal is © The Royal Society of Chemistry year

J. Mater. Chem. A, [year], **[vol.]**, 00-00 | **8**

Graphical and Textual Abstract

Alizarin (AZ) with multi-electron redox center is selected to functionalize three-dimensional self-assembled graphene hydrogels (SGHs) through non-covalent modification and the electrode material shows a good self-synergy and potential self-matching behavior.